RESEARCH PAPER

PCCP
www.rsc.org/pccp

Evidence for C_{60} dimerisation in the fulleride $[Cr(C_9H_{12})_2]^+C_{60}^-$

Andreas Hönnerscheid,[a] Leo van Wüllen,[a] Robert Dinnebier,[a] Martin Jansen,*[a] Jürgen Rahmer[b] and Michael Mehring[b]

[a] *Max-Planck-Institut für Festkörperforschung, Heisenbergstr. 1, 70569 Stuttgart, Germany. E-mail: m.jansen@fkf.mpg.de; Fax: +49 711 6891502; Tel: +49 711 6891501*

[b] *2. Physikalisches Institut, Universität Suttgart, Pfaffenwaldring 57, 70550 Stuttgart, Germany*

Received 5th January 2004, Accepted 16th February 2004
First published as an Advance Article on the web 18th March 2004

We report a detailed study of the structure, dynamics and electronic structure of the new fulleride $[Cr(C_9H_{12})_2]^+C_{60}^-$. Using a variety of characterization tools including EPR, NMR, SQUID magnetic measurements and high resolution X-ray powder diffraction a spin pairing of the C_{60}^- spins with decreasing temperatures could be observed. Contrary to the observed phase transition of first order in the related compound $[Cr(C_6H_9)_2]^+C_{60}^-$ the phase transition observed in the title compound is of higher order.

Introduction

The most characteristic feature of C_{60} is its strong electron accepting character, which can be attributed to two triply degenerate low-lying unoccupied orbitals, the three t_{1u} LUMO orbitals and the three t_{1g} LUMO + 1 orbitals. Formal ionic charges up to −12 have been realised using alkaline or alkaline-earth metals as reducing agents.[1,2] Most of the fullerides synthesised to date can structurally be described by a fcc (face centred cubic) arrangement of C_{60}^{x-} molecules with the cations in tetrahedral and/or octahedral voids.

Fullerides exhibit exceptional properties such as superconductivity[3,4] or ferromagnetism[5,6] and it would thus be very interesting to study fullerides containing transition metals instead of alkaline or alkaline-earth metals. Thus far, fullerides doped with transition metals are limited to mostly rather poorly characterised materials.[7–9] The reasons for the sparse occurence of transition-metal fullerides are on the one hand the size mismatch between the small, highly charged metal cations and the large fulleride anions. On the other hand the estimated small lattice energies of hypothetical M_xC_{60} fullerides—due to comparatively long M^{n+}–C_{60}^{n-} distances—as well as the large heats of vaporisation of common transition metals indicate thermodynamically unstable compounds. This is pointed out in Fig. 1 which shows a Born–Haber-cycle process for a hypothetical MC_{60} fulleride.

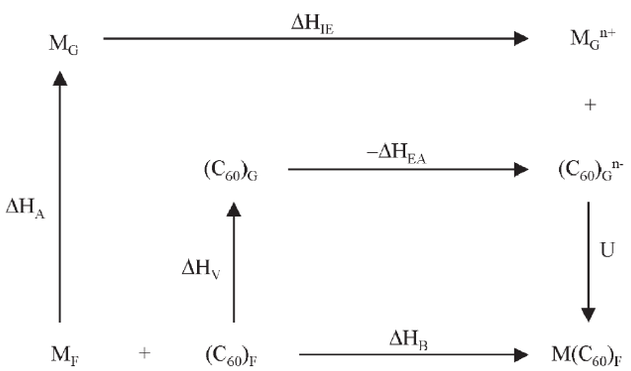

Fig. 1 Born–Haber-cycle process for a hypothetical MC_{60}-fulleride.

A promising way to counter both effects is the complexation of the transition metal, *e.g.*, with ammonia[10–12] or arene ligands.[13] This leads to bigger entities, that are more suitable to fill the voids in the C_{60}-lattice. Furthermore the thermodynamic stability is enhanced by the formation energy of the transition-metal complexes.

Recently we investigated the transition-metal fulleride $CrTol_2C_{60} = [Cr(C_7H_8)_2]C_{60}$,[14] which is an unusual compound in several respects. It consists of monoanionic C_{60} molecules in a primitive cubic (pc) arrangement with $CrTol_2^+$ cations filling the cubic voids. To our knowledge this is the first example of a fulleride that crystallises in a CsCl-type structure.

Interestingly, $CrTol_2C_{60}$ exhibits a clear reversible first order phase transition at 250 K. Upon cooling through the transition temperature a pairing of the C_{60}^- monomers into $(C_{60})_2^{2-}$ dimers was observed. This transformation was monitored and confirmed by EPR, NMR, SQUID magnetic and DSC measurements. The crystal structure of the ordered dimer-phase could be solved based on synchrotron powder diffraction data.[15]

Apart from $CrTol_2C_{60}$, there are only a few compounds containing $(C_{60})_2^{2-}$ dimers known to date. Monoanionic AC_{60}-fullerides (A = K, Rb, Cs) form metastable dimer phases upon a special temperature treatment,[16–19] as seen by ^{13}C NMR.[20] Recently, Konarev *et al.* reported on several compounds containing C_{60} or C_{70} monoanions in combination with different transition-metal complexes like $Cp^*_2Cr^+$, Cp_2Co^+ and $Cr(C_6H_6)^+$.[21,22] These compounds also exhibit $(C_{60})_2^{2-}$ dimer formation upon cooling at different temperatures. Spectroscopic results were similar to those for $CrTol_2C_{60}$. Additionally the structure of the dimer phase of $Cp^*_2CrC_{60}\cdot(C_6H_4Cl_2)_2$ has been solved by single crystal analysis.

Although the dimer-forming fullerides adopt various packing shemes, a distance of about 10 Å between adjacent fullerene centres can be identified as the common structural motif. This is the normal *van-der-Waals* distance as observed in C_{60} as well as in most alkali-metal fullerides.

In this paper we present the results on the related compound $CrMes_2C_{60} = [Cr(C_9H_{12})_2]C_{60}$. Due to the increase in size of the transition-metal complex, a corresponding increase in the interfulleride distance is expected. In the following, the properties of $CrMes_2C_{60}$ fulleride are studied in detail and related to the results on $CrTol_2C_{60}$.

DOI: 10.1039/b317060h

Experimental

C_{60} was used as purchased from the MER Company (99.9% purity). Bis(mesitylene)chromium was prepared *via* the Fischer–Hafner synthesis[23] followed by a twofold sublimation of the raw product. $CrMes_2C_{60}$ was synthesized by dropwise addition of a solution of bis(mesitylene)chromium to a solution of C_{60}, both in toluene. To agglomerate the resulting colloidal black precipitate the solvent toluene was replaced by the less polar pentane. The filtered residue was washed with pentane and dried *in vacuo*. All manipulations were performed under strictly inert conditions, because the product is sensitive to air and moisture.

Powder-diffraction patterns at room temperature have been recorded on samples sealed in a 0.3 mm capillary using a Stoe-Stadi P diffractometer, equipped with a Ge (111) primary monochromator, with copper Kα radiation ($\lambda = 154.06$ pm). The synchrotron measurements at low temperature have been carried out on the beamline X3B1 of the National Synchrotron Light Source at Brookhaven National Laboratory in transmission geometry with the sample sealed in a 0.7 mm capillary using a wavelength of 115.071 pm. Further experimental details can be found elsewhere.[24]

Magnetic susceptibility measurements have been carried out at a magnetic field of 5 T on samples sealed in quartz tubes with an MPMS 7.0 SQUID-magnetometer (Quantum Design, San Diego). The diamagnetism of the tube as well as of the reactants, C_{60} and bis(mesitylene)chromium, was measured and subtracted from the results.

EPR spectra were recorded on samples sealed in evacuated quartz tubes at X-band frequencies (9 GHz) and in high field at W-band frequencies (94 GHz). For the X-band measurements a standard Bruker spectrometer with a rectangular cavity was used. W-band measurements were carried out on a Bruker Elexsys 680 spectrometer, which was equipped with a cylindrical cavity; g values are corrected by comparison to a reference sample.

All NMR experiments were performed on a Bruker DSX 400 spectrometer operating at 9.4 T using a 7 mm MAS NMR probe at a resonance frequency of 100.61 MHz. The spectra were recorded at a spinning frequency of 4 kHz in a temperature range of 150–300 K. Repetition rates of 100 ms to 300 s were used. The chemical shift is referenced relative to TMS.

Results

Powder diffraction

The room temperature powder diffraction pattern of $CrMes_2C_{60}$ is shown in the upper part of Fig. 2. Indexing reveals a rhombohedrally centred hexagonal cell with the dimensions $a = 14.619(1)$, $c = 16.773(1)$ Å, $V = 3105(1)$ Å^3. The lattice parameters of the primitive rhombohedral cell are $a = 10.124$ Å, $\alpha = 92.44°$, $V = 1035(1)$ Å^3. The cell can be derived from the cubic one of $CrTol_2C_{60}$ ($a = 9.9883(4)$ Å, $V = 996.5(1)$ Å^3) by a small deformation along one body diagonal, corroborating the strong similarity of both structures. Possible space groups are $R\bar{3}$ and $R\bar{3}m$. The calculated powder pattern of a model of $CrMes_2C_{60}$ (space group $R\bar{3}$), which was created using the program *KPLOT*[25] is shown in the lower part of Fig. 2. For the model the six membered rings of both molecules (C_{60} and $CrMes_2$) were oriented perpendicular to the hexagonal c-axis. The orientation in the a–b-plane is arbitrary. The calculated powder pattern is almost identical to the measured one, thus confirming the validity of the model. The distance between adjacent C_{60}^- molecules at room temperature is significantly higher in $CrMes_2C_{60}$ than in $CrTol_2C_{60}$ ($\Delta a = 0.136$ Å). Synchrotron powder diffraction measurements at low temperatures reveal no structural changes for $CrMes_2C_{60}$ as observed for $CrTol_2C_{60}$. The lattice parameters at 50 K are $a = 14.459(1)$ and $c = 16.598(1)$ Å, $V = 3005(1)$ Å^3. The corresponding primitive rhombohedral cell has the dimensions $a = 10.015$ Å and $\alpha = 92.42°$, $V = 1002(1)$ Å^3. Assuming a C_{60} radius of 3.5 Å the minimum distance between adjacent carbon atoms on different C_{60} molecules is at least 3 Å, being the normal *van der Waals* distance of a close packed C_{60} lattice. In comparison, the distance between single bonded C_{60} molecules in $Cp^*_2CrC_{60}\cdot(C_6H_4Cl_2)_2$ is 9.28 Å and the corresponding dimer bond length is 1.597(7) Å.[21] Thus, the concept of dimer formation in $CrMes_2C_{60}$ at low temperatures is not supported by the powder diffraction data.

The changes in the lattice parameters (c-axis) with temperature, as obtained from temperature dependent synchrotron measurements, are plotted in Fig. 3. A noticeable deviation from a linear trend is obvious at around 190 K, indicating a phase transition of higher order.

Fig. 4 exhibits the Rietveld-plot ($R\bar{3}$) of the synchrotron data measured at 50 K. The corresponding structure is mapped

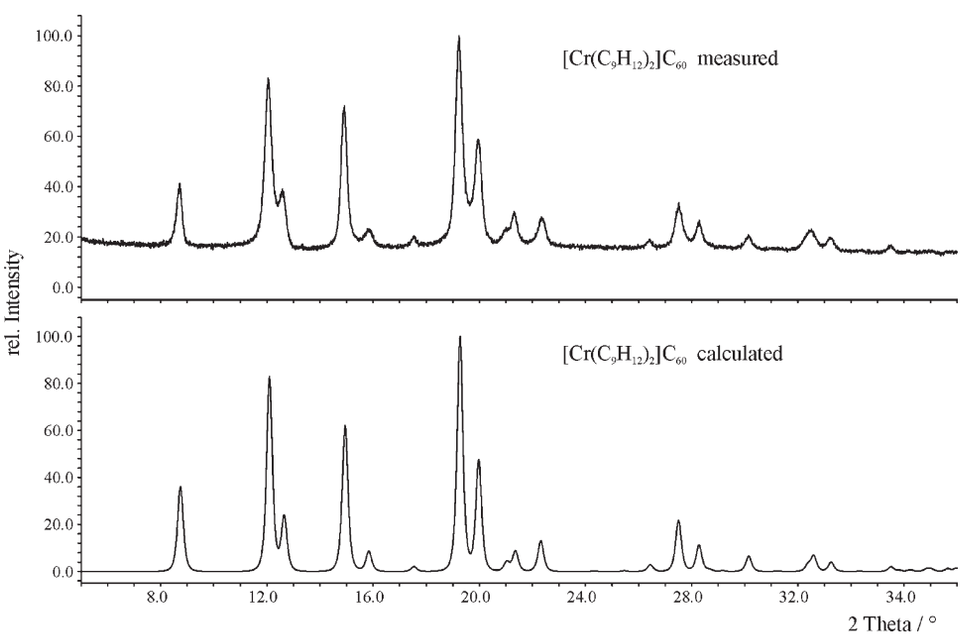

Fig. 2 Room temperature powder diffraction pattern of $CrMes_2C_{60}$. Top: experimental powder pattern; bottom: calculated powder pattern of a model of $CrMes_2C_{60}$ in space group $R\bar{3}$.

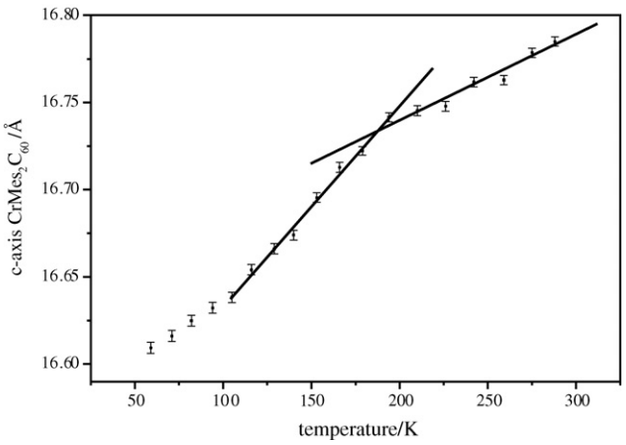

Fig. 3 Temperature dependence of the *c*-axis of the hexagonal unit cell of $CrMes_2C_{60}$.

in Fig. 5. Since the shapes of the C_{60} molecule and the $CrMes_2$ complex are known in narrow limits, both entities were introduced as rigid bodies in an orientation that is compatible to the existence of a threefold axis. Thus, the refinable parameters were reduced to one rotational parameter for each rigid body (rotation around the *c*-axis). Due to strong anisotropic peak broadening caused by microstrain together with a high background, the attainable experimental resolution is just about 2 Å. Thus, detailed structural features of $CrMes_2C_{60}$ could not be obtained. However, a significant result of the refinement is the nearly eclipsed arrangement of the six membered rings in $CrMes_2$ and C_{60} respectively, pointed out in the left part of Fig. 5. This conformation rules out $R\bar{3}m$ as a possible space group, leaving $R\bar{3}$ as the only possible solution. Further details of the refinement are listed in Table 1. To account for the anisotropic peak broadening the phenomenological model of Stephens as implemented in the program GSAS was used.[26] The resulting anisotropic microstrain distribution is visualised in Fig. 6. Regarding microstrain as an indication for compressibility along different directions, one could deduce a distinct compressibility along the *c*-direction of the unit cell, which is also the direction of the longest interfulleride distance. However, the data does not allow a complete interpretation of the microstrain distribution.

SQUID magnetic measurements

Fig. 7 plots the static inverse paramagnetic susceptibility of $CrMes_2C_{60}$ *versus* temperature. In this plot straight lines through the origin indicate Curie behaviour. For comparison the corresponding curve of $CrTol_2C_{60}$ is shown in the inset. In the range from about 170 K to 360 K the spins in $CrMes_2C_{60}$ follow a Curie–Weiss like behaviour. The slope in this temperature range translates to a magnetic moment of $\approx 2.4\ \mu_B$. Neglecting orbital contributions to the magnetization, this value is in accordance with the assumption of a system comprised of two independent unpaired electrons per formula unit. Thus, similar to the room-temperature phase of $CrTol_2C_{60}$, $CrMes_2C_{60}$ consists of bis(arene)chromium cations and C_{60} monoanions. However, in contrast to $CrTol_2C_{60}$, no corresponding phase transition is observed for $CrMes_2C_{60}$ at subambient temperatures.

At about 150 K a deviation from linearity of the $1/\chi$ *versus* T curve is obvious. It can be attributed to a successive reduction of spin carriers in $CrMes_2C_{60}$.

NMR spectroscopy

The temperature dependent ^{13}C-MAS NMR spectra of $CrMes_2C_{60}$ are compiled in Fig. 8. The room temperature spectrum exhibits a single resonance line at 183 ppm, accompanied by two rather weak spinning sidebands together with a minor signal at 143 ppm, presumably arising from a C_{60} impurity. The corresponding static ^{13}C spectrum (not shown) exhibits a signal with a line width (FWHH) of 2.4 kHz.

Upon cooling, three significant changes in the ^{13}C-MAS NMR spectra can be observed. First, the position of the ^{13}C signal shifts from 183 ppm at room temperature to 204 ppm at $T = 150$ K (*cf.* Fig. 9). This behaviour reflects the typical Curie dependence of the paramagnetic C_{60} monoanion. Second, the number and intensities of the spinning sidebands is growing considerably with decreasing temperature. The ^{13}C MAS NMR spectrum, taken at $T = 150$ K, was fitted using the Bruker Winfit software, resulting in $\delta_{iso} = 204.0$ ppm, $\Delta_{CS} = 135$ ppm, $\eta_{CS} = 0$. Third, apart from the overall broadening of the MAS spectra, a drastic broadening of the individual MAS signals (isotropic line and spinning sidebands) is obvious. This behaviour can—at least in part—be ascribed to the combined action of a temperature gradient within the MAS rotor and the temperature dependence of the ^{13}C NMR signal of $CrMes_2C_{60}$. The temperature difference between the top and the bottom of the MAS rotor was estimated using a setup in which $Pb(NO_3)_2$, a well-established chemical shift thermometer,[27] was placed on the bottom and at the top of a MAS rotor, separated by boron nitride. With this setup, the ^{207}Pb-MAS-NMR spectra, compiled in Fig. 10, resulted for the indicated temperatures.

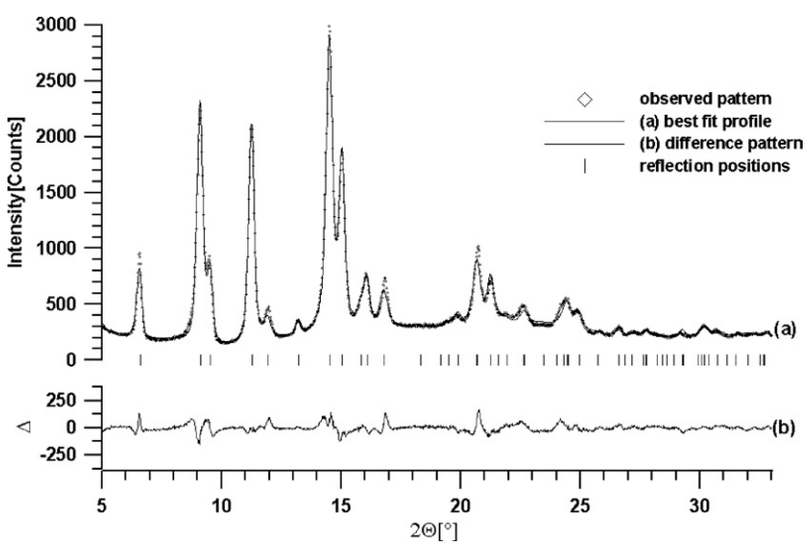

Fig. 4 Rietfeld plot of the synchrotron data for $CrMes_2C_{60}$ at 50 K.

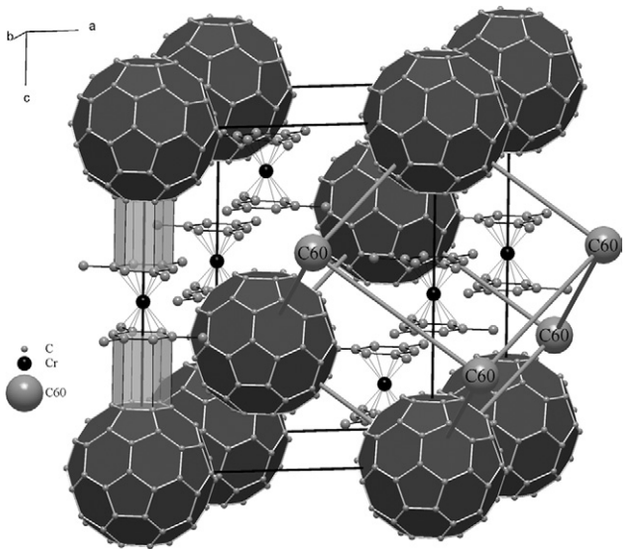

Fig. 5 Structure of $CrMes_2C_{60}$ (from Rietveld refinement of the synchrotron data taken at 50 K). Edges of the hexagonal unit cell are in black, the corresponding edges of the primitive rhombohedral cell are in grey. The nearly eclipsed conformation of the six membered rings—of C_{60} and $CrMes_2$ respectively—is pointed out on the left side.

The temperature difference between the top and bottom end of the MAS rotor can be calculated using the relation $\Delta T \approx 1.3\ \Delta\delta_{CS}$[28] allowing for an estimation of the temperature-gradient induced line broadening for the ^{13}C-NMR signal of $CrMes_2C_{60}$. At $T = 157$ K, the temperature difference amounts to 12 K, which translates into a ^{13}C line width of 4 ppm.

EPR spectroscopy

CW EPR spectra of $CrMes_2C_{60}$ were obtained at X-band (9.5 GHz) and W-band (95 GHz) frequencies in the temperature range 6–100 K using Li:LiF as a *g*-factor reference sample. At X-band a symmetric line of Lorentzian character was observed which narrows from 5.7 mT at room temperature to 2.3 mT at 40 K. The temperature dependence of the line position is shown in Fig. 11. At W-band frequencies, the EPR line is considerably broadened already at room temperature and broadens further with decreasing temperature (see Fig. 12). The lineshape becomes progressively asymmetric with decreasing temperature. At 6 K the *g* anisotropy is fully developed. At this temperature the observed *g*-factor of $g = 1.9888$ corresponds to the $CrMes_2^+$ complex.

Table 1 Crystallographic data for the low temperature phase of $Cr(C_9H_{12})_2C_{60}$. R-p, R-wp, R-F, and R-F^2 refer to the Rietveld criteria of fit for profile and weighted profile respectively, defined in the GSAS manual

Formula	$C_{60}Cr(C_9H_{12})_2$
Temperature/K	50
Formula weight/g mol−1	3092.809
Space group	$R\bar{3}$
Z	3
a/Å	14.4590(7)
c/Å	16.5981(21)
V/Å^3	3005.2(4)
ρ_{calc}/g cm^{-3}	1.709
2Θ range/°	5–33.0
2Θ step size/°	0.02
Wavelength/Å	1.1507(2)
μ/cm^{-1}	12.36
R_p (%)	4.99
R_{wp} (%)	5.44
R_F (%)	3.81
R_{F^2} (%)	5.64
No. of reflections	83

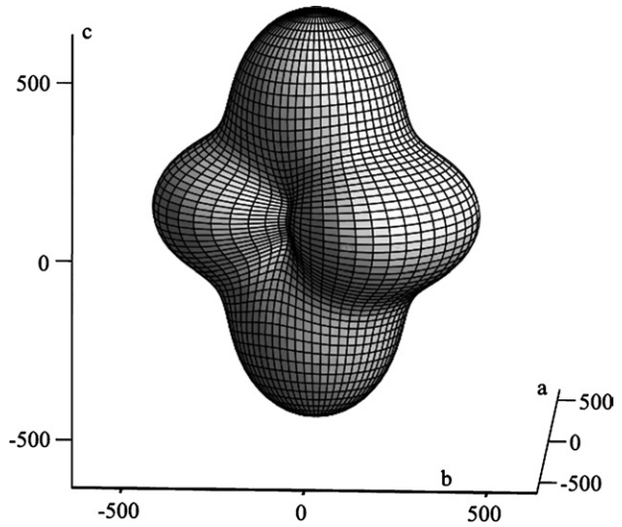

Fig. 6 3-Dimensional representation of the isosurface of the fourth order microstrain tensor of $CrMes_2C_{60}$ at 50 K.

Discussion

The combined results allow for a detailed discussion of the dynamics and electronic structure in $CrMes_2C_{60}$. The reduced mobility of the C_{60} entities with decreasing temperature in combination with the observed reduction of spin carriers are in tune with a thermally activated dimer formation. At room temperature the situation can be described as isolated C_{60}^- monoanions which can perform reorientational motion. The NMR line width of the static room temperature ^{13}C NMR spectrum hints at a partially averaged CSA tensor due to reorientational motion of the C_{60} cages. The chemical shift of 183 ppm at room temperature confirms the presence of monoanionic C_{60} species, the downfield shift of approx. 40 ppm relative to pristine C_{60} predominantly arises from a paramagnetic shift. This is corroborated by the temperature dependence of the isotropic chemical shift of this signal which follows a Curie like behaviour (*cf.* Fig. 9). The observation of a single EPR line with a *g* value of 1.9925 indicates an exchange coupled spin system at room temperature with a spin $\frac{1}{2}$ on every C_{60}^- and another one on the mesitylene chromium complex. Decreasing

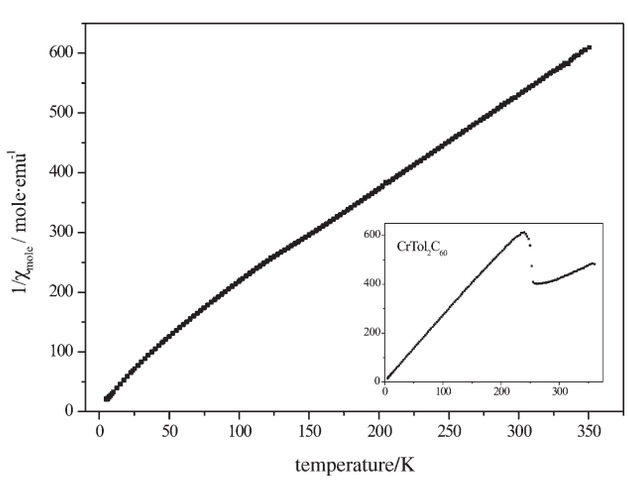

Fig. 7 SQUID magnetic measurement of $CrMes_2C_{60}$ ($B = 5$ T). Plotted is the inverse susceptibility as a function of temperature. The insert shows the corresponding graph for $CrTol_2C_{60}$.

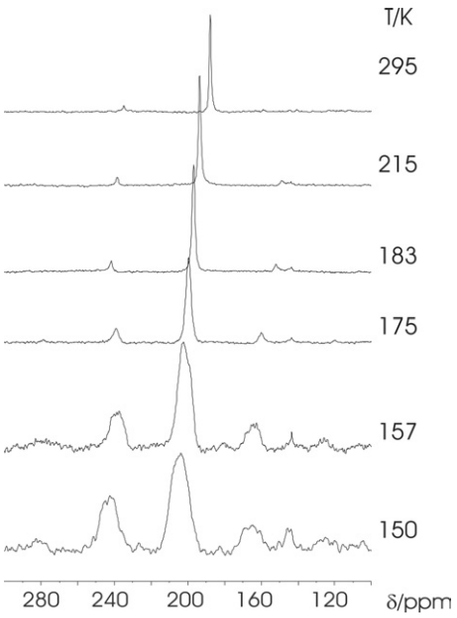

Fig. 8 Temperature dependence of the ^{13}C MAS NMR spectra of $CrMes_2C_{60}$.

the temperature leads to an increase in the spinning sideband intensity, reflecting a successive slowing down of the reorientational motion of the C_{60} cage. At $T = 150$ K, the width of the CSA tensor ($\Delta_{CS} = 135$ ppm, $\eta_{CS} = 0$, obtained from a Herzfeld–Berger analysis of the spinning sidebands[29]) compares well to that of the ^{13}C signal of immobile C_{60} cages in pristine C_{60}[30] at $T = 113$ K. Since no lower temperatures are accessible with our equipment, no ^{13}C NMR spectra could be obtained in the temperature range 150 K–25 K. Therefore, we cannot unequivocally decide whether the C_{60} cages are completely static at $T = 150$ K or if the freezing of the motion is not fully complete at this temperature. However, the width of the CSA tensor indicates a reorientational frequency $<10^4$ Hz for the reorientation.[31]

It is quite important to note that the chemical shift of the more or less static C_{60} cages still contain the paramagnetic contribution (downfield shift relative to C_{60}), thus excluding immediate complete spin pairing upon immobilisation, as observed in the related $CrTol_2C_{60}$.

For a discussion of the effects occurring at even lower temperatures, we have to resort to the results of the EPR and SQUID magnetic measurements. When lowering the temperature the EPR spectrum gradually develops into a spectrum indicative of a single spin system characteristic of only the

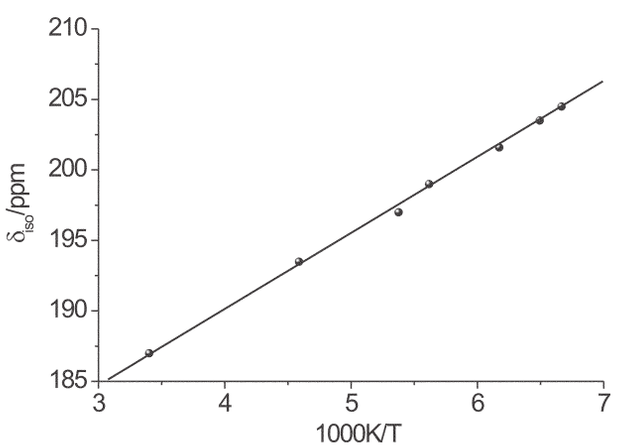

Fig. 9 Temperature dependence of the chemical shift of the central ^{13}C MAS NMR signal of $CrMes_2C_{60}$.

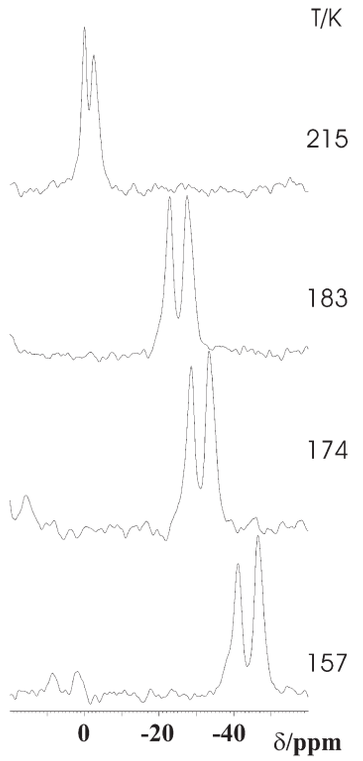

Fig. 10 ^{207}Pb MAS NMR spectra of $Pb(NO_3)_2$ at different temperatures (for details see text).

$CrMes_2^+$ complex at low temperatures. This scenario is supported by the temperature dependence of the total susceptibility (Fig. 7) and the average *g*-factor (Fig. 11). We note in addition that also the *g*-factor at 6 K corresponds entirely to the $CrMes_2^+$ complex. In this respect the behaviour resembles that of $CrTol_2C_{60}$ with the difference that there is an abrupt change of the susceptibility (Fig. 7) and the *g*-factor (Fig. 11) occurring at 250 K. Around this temperature also the EPR lineshape (at W-band) changed abruptly whereas in the case discussed here the change is monotonic over the whole temperature range which also holds for the temperature dependence of the *g*-factor (Fig. 11).

Thus, the material consists of a $CrMes_2^+C_{60}^-$ complex with two exchange coupled spin $\frac{1}{2}$ at room temperature and only a single spin $\frac{1}{2}$ on $CrMes_2^+$ and no spin on C_{60} at low temperatures. Furthermore there is no evidence for a phase transition from the EPR data. Both the gradual change of the *g*-factor

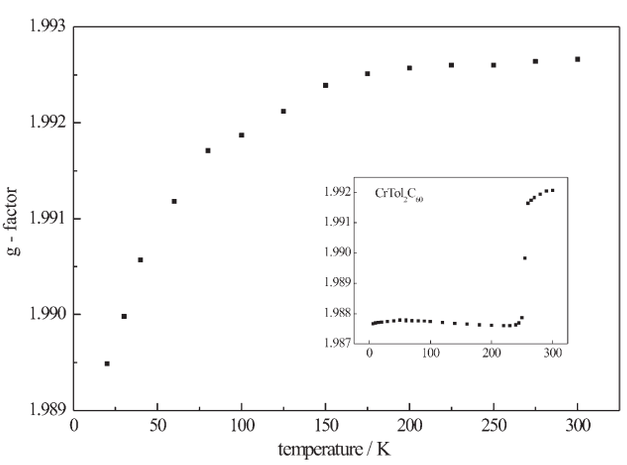

Fig. 11 Temperature dependence of the isotropic *g*-value of $CrMes_2C_{60}$ (X band). The inset shows the corresponding graph for $CrTol_2C_{60}$.

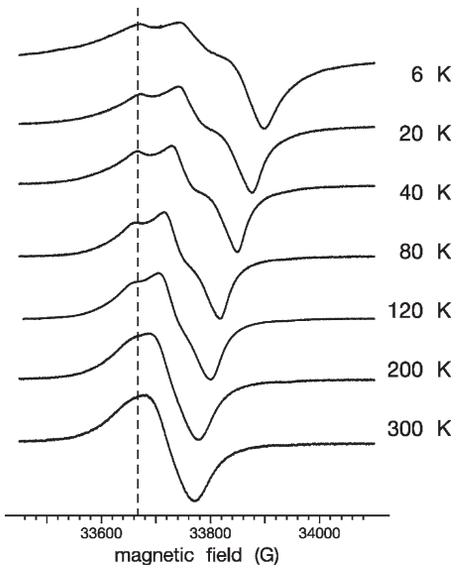

Fig. 12 W-band EPR spectra of $CrMes_2C_{60}$ as a function of temperature.

and the lineshape can consistently be explained by a model which assumes a spin pairing of the C_{60}^- spins, possibly by dimer formation, at low temperature and a thermally activated bond breaking with increasing temperature. Assuming a Curie susceptibility for the C_{60}^- spins allows to extract from the temperature dependence of the total *g*-factor (Fig. 11) the number of C_{60}^- spins at different temperatures (*cf.* Fig. 13). The observed behaviour can be described by a Boltzmann law with activation energy $\Delta E/k = 62.5$ K as:

$$n_{60} = n_{60}e^{-\Delta E/kT}$$

where n_{60} is the number of spin carrying C_{60}^- molecules and n_0 their total number.

From a solid state point of view the observation of a diamagnetic ground state (with one electron per C_{60} molecule on average) and the thermally activated increase of the magnetic susceptibility can only be reconciled by a gap opening when lowering the temperature. This excludes an antiferromagnetic ground state and is evidence for a spin paired state at low temperatures. The gap between the diamagnetic ground state and the paramagnetic state is manifested by the activation energy. It is reminiscent of a spin Peierls or ordinary Peierls transition. This, however, is just a speculation and further evidence is required.

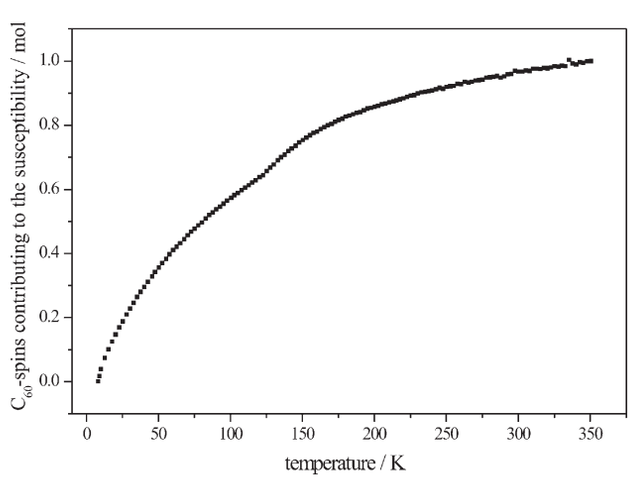

Fig. 13 Number of C_{60} spins extracted from the temperature dependence of the total *g*-factor. (for details see text).

Both types of Peierls transitions are accompanied by a periodic lattice distortion which for commensurability reasons would in this case be a dimerization. It is well known that the lattice distortion can be very small and is in general detected only by diffuse X-ray scattering. It is therefore not surprising that it has not been seen in the applied XRD. Further investigations are required to verify this conjecture.

Conclusion

The temperature dependent changes of the electronic structure and the dynamics in the new fulleride $CrMes_2C_{60}$ could be successfully studied using a combined approach using EPR, NMR, SQUID magnetic measurements and X-ray powder diffraction techniques. While the situation at ambient temperatures and very low temperatures resemble those found for the related $CrTol_2C_{60}$ — an exchange coupled spin system at room temperature with rapidly reorienting C_{60} cages and a single spin system with the electron spin localized on the $CrMes_2^+$ complex with static, non-reorienting C_{60} cages at low temperatures — the transition between these two extreme states is completely different in these two samples. The transition in $CrTol_2C_{60}$ is observed to be of first order with clear evidence for a dimer formation at the transition temperature of 250 K. The transition in $CrMes_2C_{60}$, on the other hand, is obviously of higher order and might be due to some type of Peierls transition. Further evidence is required to verify this. The reason for the different behaviour is to be found in the larger C_{60}–C_{60} distances, induced by the larger chromium complex in $CrMes_2C_{60}$ which inhibits spontaneous dimer formation upon freezing of the C_{60} reorientation.

References

1 A. R. Kortan, N. Kopylov, S. Glarum, E. M. Gyorgy, A. P. Ramirez, R. M. Fleming, O. Zhou, F. A. Thiel, P. L. Trevor and R. C. Haddon, *Nature*, 1992, **360**, 566.
2 L. Cristofolini, M. Ricco and R. De Renzi, *Phys. Rev. B: Condens. Matter*, 1999, **59**, 8343.
3 A. F. Hebard, M. J. Rosseinsky, R. C. Haddon, D. W. Murphy, S. H. Glarum, T. T. M. Palstra, A. P. Ramirez and A. R. Kortan, *Nature*, 1991, **350**, 600.
4 K. Holczer, O. Klein, S. M. Huang, R. B. Kaner, K. J. Fu, R. L. Whetten and F. Diederich, *Science*, 1991, **252**, 1154.
5 P. M. Allemand, K. C. Khemani, A. Koch, F. Wudl, K. Holczer, S. Donovan, G. Gruner and J. D. Thompson, *Science*, 1991, **253**, 301.
6 P. W. Stephens, D. Cox, J. W. Lauher, L. Mihaly, J. B. Wiley, P. M. Allemand, A. Hirsch, K. Holczer, Q. Li, J. D. Thompson and F. Wudl, *Nature*, 1992, **355**, 331.
7 L. Qian, L. Norin, J. H. Guo, C. Sathe, A. Agui, U. Jansson and J. Nordgren, *Phys. Rev. B: Condens. Matter*, 1999, **59**, 12 667.
8 V. Venegas, J. Ortiz-Lopez, G. Rueda-Morales and F. Caleyo, *Chem. Phys. Lett.*, 2000, **318**, 655.
9 C. Bossard, S. Rigaut, D. Astruc, M. H. Delville, G. Félix, A. Février-Bouvier, J. Amiell, S. Flandrois and P. Delhaès, *Chem. Commun.*, 1993, 333.
10 K. Himmel and M. Jansen, *Chem. Commun.*, 1998, **7**, 1205.
11 K. Himmel and M. Jansen, *Eur. J. Inorg. Chem.*, 1998, **8**, 1183.
12 H. Brumm and M. Jansen, *Z. Anorg. Allg. Chem.*, 2001, **627**, 1433.
13 W. E. Broderick, K. W. Choi and W. C. Wan, *Proc. - Electrochem. Soc.*, 1997, **14**, 1102.
14 A. Hönnerscheid, L. van Wullen, M. Jansen, J. Rahmer and M. Mehring, *J. Chem. Phys.*, 2001, **115**, 7161.
15 A. Hönnerscheid, R. Dinnebier and M. Jansen, *Acta Crystallogr., Sect. B: Struct. Sci.*, 2002, **B58**, 482.
16 Q. Zhu, D. E. Cox and J. E. Fischer, *Phys. Rev. B: Condens. Matter*, 1995, **51**, 3966.
17 G. Oszlanyi, G. Bortel, G. Faigel, M. Tegze, L. Granasy, S. Pekker, P. W. Stephens, G. Bendele, R. Dinnebier, G. Mihaly, A. Janossy, O. Chauvet and L. Forro, *Phys. Rev. B: Condens. Matter*, 1995, **51**, 12 228.

18 M. Kosaka, K. Tanigaki, T. Tanaka, T. Atake, A. Lappas and K. Prassides, *Phys. Rev. B: Condens. Matter*, 1995, **51**, 12 018.
19 G. Oszlanyi, G. Bortel, G. Faigel, L. Granasy, G. M. Bendele, P. W. Stephens and L. Forro, *Phys. Rev. B: Condens. Matter*, 1996, **54**, 11 849.
20 K.-F. Thier, F. Rachdi and M. Mehring, *Phys. Rev. B: Condens. Matter*, 1997, **55**, 124.
21 D. V. Konarev, S. S. Khasanov, A. Otsuka and G. Saito, *J. Am. Chem. Soc.*, 2002, **124**, 8520.
22 D. V. Konarev, S. S. Khasanov, G. Saito, A. Otsuka, Y. Yoshida and R. N. Lyubovskaya, *J. Am. Chem. Soc.*, 2003, **125**, 10 074.
23 E. O. Fischer, S. Schreiner and A. Reckziegel, *Chem. Ber.*, 1961, **94**, 258.
24 R. E. Dinnebier, W. A. Dollase, X. Helluy, J. Kummerlen, A. Sebald, M. U. Schmidt, S. Pagola, P. W. Stephens and S. van Smaalen, *Acta Crystallogr., Sect. B: Struct. Sci.*, 1999, **B55**, 1014.
25 R. Hundt, *KPLOT. A Program for Plotting and Investigating Crystal Structures, updated version 6.4.1.,*Univ. Bonn, Germany, 1979.
26 P. W. Stephens, *J. Appl. Crystallogr.*, 1999, **32**, 281.
27 A. Bielecki and D. P. Burum, *J. Magn. Reson., Ser. A*, 1995, **116**, 215.
28 T. Takahashi, H. Kawashima, H. Sugisawa and T. Baba, *Solid State Nucl. Magn. Reson.*, 1999, **15**, 119.
29 J. Herzfeld and A. E. Berger, *J. Chem. Phys.*, 1980, **73**, 6021.
30 R. Tycko, G. Dabbagh, R. M. Fleming, R. C. Haddon, A. V. Makhija and S. M. Zahurak, *Phys. Rev. Lett.*, 1991, **67**, 1886.
31 U. Kessler, L. van Wullen and M. Jansen, *Inorg. Chem.*, 2001, **40**, 7040.

